An Obliquely Incident Wave Propagation Through the Jointed Complex Rock Masses

Yexue Li[1], Yuanyuan Wang[1], Yu Cheng[1], and Jinshun Xue[1]

[1]School of Civil Engineering and Architecture, Hubei University of Arts and Science, Xiangyang City, China
E-mail: warmhearted520@163.com

ABSTRACT: Based on the wave function, the stresses and particle displacements on the joint are derived when the incident P-wave and S-wave are obliquely incident to the jointed complex rock masses. And then, a modified time domain recursive method (MTDRM) is proposed. Based on the MTDRM, this paper investigates the P-wave and S-wave propagation crossing the jointed complex rock masses. The effects of the wave impedance ratios and the incident angles on the transmission and reflection coefficients are discussed. It is found that the wave crossing the jointed complex rock masses is not always attenuated but may be strengthened in some special cases.

KEYWORDS: Modified time domain recursive method, Jointed complex rock masses, Wave impedance ratio, Wave propagation.

1. INTRODUCTION

It is well known that natural rock masses contain many discontinuous interfaces, such as joints, pores, and fractures. When a seismic wave propagates through the discontinuous interfaces, it suffers energy dissipation and waveform changing (Li et al., 2018; Che et al., 2016). Finally, the seismic wave acting on the building and infrastructure will result in huge losses and damages. If we have deep knowledge towards the wave propagation, some suitable parameters can be proposed to design the building with better antiseismic properties. And the loss can be reduced when the building encounters an earthquake. Unfortunately, it is still far from complete for us to understand the wave propagation through the jointed rock masses.

Also, although many novel methods for the underground cavern excavation emerge in an endless stream, blasting is still the usual method for mineral mining so far (Zeng et al., 2018). A blasting wave starts from the explosion source and gradually transfers into a stress wave due to the energy attenuation. When the stress wave encounters the joint, the complex transmission and reflection take place (Li et al., 2011). The complex stress fields formed by the superposition of the transmitted and reflected waves are easier to cause the surrounding rock damage and even the structural collapse (Deng et al., 2014). Thus, from the above two engineering contents, it is important to study the stress wave propagation crossing the joint.

In the previous studies, in order to simplify the problem, the stress wave is assumed to be perpendicular to the joint (Li and Wang, 2019; Zhu et al., 2011), which avoids the wave mode conversion. The usual method for investigating the wave which is normally incident to the joint is the characteristic method. Using this method, the wave propagation through the linearly elastic joint is studied (Cai and Zhao, 2000; Zhao et al., 2006). Subsequently, the interactions of the stress waves with the nonlinear joint (Zhao and Cai, 2001; Fang and Yong, 2013) and the viscoelastic joint (Zhao and Cai, 2001) are studied.

In a word, the characteristic method is effective to study the normally incident wave propagation. However, it is very difficult for the characteristic method to investigate the obliquely incident wave propagation. Many methods have been proposed and applied for solving the problem of an obliquely incident stress wave interacting with the joint, including the equivalent medium method (Li et al., 2010; Li and Zhu, 2012), the scattering matrix method (Perino et al., 2012; Perino et al., 2010), the virtual wave source method (Zhu and Zhao, 2013). Li and Ma (2010) also proposed a novel method named the time domain recursive method (TDRM). By using TDRM, the linearly elastic constitutive relationship is applied in the normal and tangential direction. The displacement discontinuity model (Schoenberg, 1983; Kitsunezaki, 1983) is introduced as the boundary condition, and finally, the particle velocity wave recursive equations are established. The relations between the transmission and reflection coefficients, wave frequency, and joint stiffness are analyzed. In fact, if the wave with a relatively large amplitude leads to the nonlinear

deformation of the joint, it is not feasible to select the linear constitutive relationship for the joint. Some investigators (Song et al., 2012; Li, 2013) applied the nonlinear constitutive relationship in the normal direction of the joint, i.e., BB model (Bandis et al.,1983; Bandis et al., 1985), to study the effect of the joint stiffness on the wave propagation. However, the above studies do not take into account the effect of the joint filling. Usually, the natural joints contain many fillings. Just because of the fillings, the displacement discontinuity cannot be satisfied any longer (Zhu et al., 2011). And the stresses in the two interfaces of the joint are discontinuous. Thus, by applying the stress discontinuity model, Zou et al. (2017) investigated the effects of the fillings on the transmission and reflection coefficients when the incident waves obliquely impinge the joints. In order to further discuss the joint viscoelastic deformation behavior caused by the filling, a more complex constitutive relationship, i.e., the standard linear solid (SLS) model, is used to characterize the stress and strain relation of the joint (Wang et al., 2017). And the wave equations, in this case, were derived.

The above studies are based on the assumption that the rock properties on the left and right interfaces of the joint are the same. As a matter of fact, in nature, the rocks on the left and right interfaces of the joint have different characteristics. The rock property differences cause wave refraction. From Snell's law, the transmitted angle is not equal to the incident angle any longer, and the reflected angle of the reflected P-wave is not equal to the reflected angle of the reflected S-wave neither. Although Fan et al. (2018) investigated the P-wave normally incident to the jointed complex rock masses by the characteristic method, the problem for the wave obliquely incident to the joint is more complicated than that for the normally incident case. Therefore, based on the wave function, a modified time domain recursive method (MTDRM) is proposed in this paper. And then using this method, the P- and S-wave propagations crossing the jointed complex rock masses with the arbitrary incident angles are investigated.

2. A MODIFIED TIME DOMAIN RECURSIVE METHOD

2.1 The Stresses and Particle Velocities of the Joint Impinged By an Incident P-Wave

The whole space is separated into two half-spaces by the joint interfaces (see Figure 1). The half-space before the joint is zone I, and the other half-space is zone II. When the obliquely incident planar P-wave or S-wave impinges the jointed complex rock masses, four separate waves are generated. i.e., reflected P-wave and S-wave and transmitted P-wave and S-wave (Nakagawa et al., 2000). Their corresponding emergence angles are α_1, β_1, α_2, β_2, respectively. Usually, the rock properties on the left and right interfaces of the joint are different. Thus, from Snell's law, the four angles are not equal to each other. The incident wave propagation direction is assumed to be

in the x-y plane and the joint interfaces to be in the y-z plane. In the coordinate system, the five stress wave functions can be uniformly expressed as:

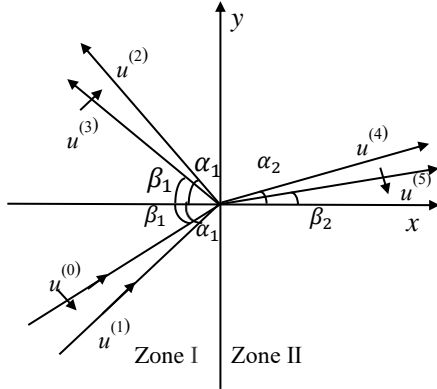$$u^{(i)}=A^{(i)}exp\left[j\left(k_x^{(i)}x+k_y^{(i)}y-\omega t\right)\right] \tag{1}$$

Figure 1 Schematic of reflected and transmitted P-wave and S-wave caused by incident P-wave or S-wave

where A is the amplitude; u is the displacement; j is the Imaginary unit; k is the wave vector; ω is the angular frequency; superscript i is equal to 0~5, and each value from 0 to 5 corresponds to the incident S-wave, the incident P-wave, the reflected P-wave and S-wave, the transmitted P-wave and S-wave, respectively. The components of the wave vector in the x, y directions are:

$$\left.\begin{array}{ll} k_x^{(1)}=\frac{\omega}{C_{P1}}cos\alpha_1 & k_y^{(1)}=\frac{\omega}{C_{P1}}sin\alpha_1 \\ k_x^{(2)}=-\frac{\omega}{C_{P1}}cos\alpha_1 & k_y^{(2)}=\frac{\omega}{C_{P1}}sin\alpha_1 \\ k_x^{(3)}=-\frac{\omega}{C_{S1}}cos\beta_1 & k_y^{(3)}=\frac{\omega}{C_{S1}}sin\beta_1 \\ k_x^{(4)}=\frac{\omega}{C_{P2}}cos\alpha_2 & k_y^{(4)}=\frac{\omega}{C_{P2}}sin\alpha_2 \\ k_x^{(5)}=\frac{\omega}{C_{S2}}cos\beta_2 & k_y^{(5)}=\frac{\omega}{C_{S2}}sin\beta_2 \end{array}\right\} \tag{2}$$

where C_{P1}, C_{S1}, C_{P2}, C_{S2} are the P-wave and S-wave velocities in the rocks before and after the joint, respectively. The displacements are discomposed along the x, y directions, and then the following equations can be obtained:

$$\left.\begin{array}{ll} u_x^{(1)}=u^{(1)}cos\alpha_1 & u_y^{(1)}=u^{(1)}sin\alpha_1 \\ u_x^{(2)}=-u^{(2)}cos\alpha_1 & u_y^{(2)}=u^{(2)}sin\alpha_1 \\ u_x^{(3)}=u^{(3)}sin\beta_1 & u_y^{(3)}=u^{(3)}cos\beta_1 \\ u_x^{(4)}=u^{(4)}cos\alpha_2 & u_y^{(4)}=u^{(4)}sin\alpha_2 \\ u_x^{(5)}=u^{(5)}sin\beta_2 & u_y^{(5)}=-u^{(5)}cos\beta_2 \end{array}\right\} \tag{3}$$

The rock is assumed to be linearly elastic. The constitutive relationship of the rock can be expressed as:

$$\sigma_{xx}=(\lambda+2\mu)\frac{\partial u_x}{\partial x}+\lambda\frac{\partial u_y}{\partial y} \tag{4}$$

$$\sigma_{xy}=\mu\left(\frac{\partial u_x}{\partial y}+\frac{\partial u_y}{\partial x}\right) \tag{5}$$

where λ, μ are Lame constants. Let $\varphi^{(i)}=k_x^{(i)}x+k_y^{(i)}y-\omega t$. In the left interface of the joint the normal and shear stresses triggered by the incident P-wave are:

$$\sigma_{xx}^{(1)}=(\lambda+2\mu)\frac{\partial u_x^{(1)}}{\partial x}+\lambda\frac{\partial u_y^{(1)}}{\partial y}$$

$$=(\lambda+2\mu)cos\alpha_1A^{(1)}exp[j\varphi^{(1)}]jk_x^{(1)}+\lambda sin\alpha_1A^{(1)}exp[j\varphi^{(1)}]jk_y^{(1)}$$

$$=(\lambda+2\mu)cos\alpha_1A^{(1)}exp[j\varphi^{(1)}]j\frac{\omega}{C_{P1}}cos\alpha_1$$

$$\quad +\lambda sin\alpha_1A^{(1)}exp[j\varphi^{(1)}]j\frac{\omega}{C_{P1}}sin\alpha_1$$

$$=A^{(1)}exp[j\varphi^{(1)}]j\omega\left[(\lambda+2\mu)cos\alpha_1\frac{cos\alpha_1}{C_{P1}}+\lambda sin\alpha_1\frac{sin\alpha_1}{C_{P1}}\right]$$

$$=\frac{v^{(1)}}{C_{P1}}(\lambda+2\mu cos\alpha_1) \tag{6}$$

Substituting the material parameters $\lambda+2\mu=\rho C_P^2$ and $\mu=\rho C_S^2$ into Eq. (6), and then one can obtain:

$$\sigma_{xx}^{(1)}=\rho C_P v\left(1-2sin^2\alpha_1\left(\frac{C_{S1}^2}{C_{P1}^2}\right)\right) \tag{7}$$

According to the conservation of momentum on the wave front, there is $\sigma = \rho C v$. Also, from Snell's law, there is:

$$\frac{sin\beta_1}{sin\alpha_1}=\frac{C_{S1}}{C_{P1}}=\sqrt{\frac{1-2v}{2(1-v)}} \tag{8}$$

From Eq. (8), Eq.(7) can be rewritten as:

$$\sigma_{xx}^{(1)}=\sigma^{(1)}cos2\beta_1 \tag{9}$$

Furthermore, in the tangential direction the shear stresses are:

$$\sigma_{xy}^{(1)}=\mu\left(\frac{\partial u_x^{(1)}}{\partial y}+\frac{\partial u_y^{(1)}}{\partial x}\right)$$

$$=\mu\left[\begin{array}{l} cos\alpha_1A^{(1)}exp[j\varphi^{(1)}]j\frac{\omega}{C_{P1}}sin\alpha_1 \\ +sin\alpha_1A^{(1)}exp[j\varphi^{(1)}]j\frac{\omega}{C_{P1}}cos\alpha_1 \end{array}\right]$$

$$=\frac{v^{(1)}}{C_{P1}}\mu sin2\alpha_1 = \sigma^{(1)}2sin^2\beta_1cot\alpha_1 \tag{10}$$

Similarly, on the left and right interfaces of the joint, the normal and tangential stresses triggered by the other waves can be expressed as:

$$\left.\begin{array}{ll} \sigma_{xx}^{(2)}=\sigma^{(2)}cos2\beta_1 & \sigma_{xy}^{(2)}=-\sigma^{(2)}2sin^2\beta_1cos\alpha_1 \\ \sigma_{xx}^{(3)}=-\sigma^{(3)}sin2\beta_1 & \sigma_{xy}^{(3)}=-\sigma^{(3)}cos2\beta_1 \\ \sigma_{xx}^{(4)}=\sigma^{(4)}cos2\beta_2 & \sigma_{xy}^{(4)}=\sigma^{(4)}2sin^2\beta_2cot\alpha_2 \\ \sigma_{xx}^{(5)}=\sigma^{(5)}sin2\beta_2 & \sigma_{xy}^{(5)}=-\sigma^{(5)}cos2\beta_2 \end{array}\right\} \tag{11}$$

The rock is assumed to be linearly elastic. The stress satisfies the superposition principle. After the stress components on the two interfaces of the joint are added, respectively, the stresses on the left interface of the joint can be expressed as:

$$\sigma^-=\sigma_{xx}^{(1)}+\sigma_{xx}^{(2)}+\sigma_{xx}^{(3)}$$

$$=\sigma^{(1)}cos2\beta_1+\sigma^{(2)}cos2\beta_1-\sigma^{(3)}sin2\beta_1 \tag{12}$$

$$\tau^-=\sigma_{xy}^{(1)}+\sigma_{xy}^{(2)}+\sigma_{xy}^{(3)}$$

$$=\sigma^{(1)}2sin^2\beta_1cot\alpha_1-\sigma^{(2)}2sin^2\beta_1cos\alpha_1-\sigma^{(3)}cos2\beta_1 \tag{13}$$

The stresses on the right interface of the joint can be expressed as:

$$\sigma^+=\sigma_{xx}^{(4)}+\sigma_{xx}^{(5)}=\sigma^{(4)}cos2\beta_2+\sigma^{(5)}sin2\beta_2 \tag{14}$$

$$\tau^+=\sigma_{xy}^{(4)}+\sigma_{xy}^{(5)}=\sigma^{(4)}2sin^2\beta_2cot\alpha_2-\sigma^{(5)}cos2\beta_2 \tag{15}$$

9

The normal and tangential components of the particle displacements on the left interface of the joint can be expressed as:

$$u_n^-=u^{(1)}cos\alpha_1-u^{(2)}cos\alpha_1+u^{(3)}sin\beta_1 \tag{16}$$

$$u_\tau^-=u^{(1)}sin\alpha_1+u^{(2)}sin\alpha_1+u^{(3)}cos\beta_1 \tag{17}$$

The normal and tangential components of the particle displacements on the right interface of the joint can be expressed as:

$$u_n^+=u^{(4)}cos\alpha_2+u^{(5)}sin\beta_2 \tag{18}$$

$$u_\tau^+=u^{(4)}sin\alpha_2-u^{(5)}cos\beta_2 \tag{19}$$

2.2 The Stresses and Particle Velocities of the Joint Impinged by an Incident S-Wave

When an S-wave impinges the joint, there are four waves emitted from the joint. They are the transmitted P- and S-wave and the reflected P- and S-wave, respectively. Similarly, the stresses on the two interfaces of the joint can be solved analogous to the solution method for the incident P-wave. The incident S-wave wave function can be written as:

$$u^{(0)}=A^{(0)}exp\left[j\left(k_x^{(0)}x+k_y^{(0)}y-\omega t\right)\right] \tag{20}$$

where $k_x^{(0)}=\frac{\omega}{C_{S1}}cos\beta_1$ $k_y^{(0)}=\frac{\omega}{C_{S1}}sin\beta_1$

The displacement components along the x and y directions are:

$$u_x^{(0)}=u^{(0)}sin\beta_1 \quad u_y^{(0)}=-u^{(0)}cos\beta_1 \tag{21}$$

Thus, on the interfaces of the joint the normal stresses triggered by the incident S-wave can be written as:

$$\begin{aligned}\sigma_{xx}^{(0)}&=(\lambda+2\mu)\frac{\partial u_x^{(0)}}{\partial x}+\lambda\frac{\partial u_y^{(0)}}{\partial y}\\&=(\lambda+2\mu)sin\beta_1 A^{(0)}exp[j\varphi^{(0)}]j\frac{\omega}{C_{S1}}cos\beta_1\\&\quad+\lambda\left(-cos\beta_1\right)A^{(0)}exp[j\varphi^{(0)}]j\frac{\omega}{C_{S1}}sin\beta_1\\&=\frac{v^{(0)}}{C_{S1}}\mu(jn2\beta_1)=\sigma^{(0)}sin2\beta_1\end{aligned} \tag{22}$$

On the interfaces of the joint the tangential stresses triggered by the incident S-wave can be written as:

$$\begin{aligned}\sigma_{xy}^{(0)}&=\mu\left(\frac{\partial u_x^{(0)}}{\partial y}+\frac{\partial u_y^{(0)}}{\partial x}\right)\\&=\mu\left[\begin{array}{l}sin\beta_1 A^{(0)}exp[j\varphi^{(0)}]j\frac{\omega}{C_{S1}}sin\beta_1\\+\left(-cos\beta_1\right)A^{(0)}exp[j\varphi^{(0)}]j\frac{\omega}{C_{S1}}cos\beta_1\end{array}\right]\\&=\frac{v^{(0)}}{C_{S1}}\mu(-cos2\beta_1)=-\sigma^{(0)}cos2\beta_1\end{aligned} \tag{23}$$

The other stresses triggered by the incident S-wave are the same as those in Eq.(11). The stress components in the left and right interfaces of the joint are superposed to obtain the corresponding normal and tangential stresses. Therefore, the normal and tangential stresses in the left interface of the joint are:

$$\sigma^-=\sigma_{xx}^{(0)}+\sigma_{xx}^{(2)}+\sigma_{xx}^{(3)}=\sigma^{(0)}sin2\beta_1+\sigma^{(2)}cos2\beta_1-\sigma^{(3)}sin2\beta_1 \tag{24}$$

$$\tau^-=\sigma_{xy}^{(0)}+\sigma_{xy}^{(2)}+\sigma_{xy}^{(3)}=-\sigma^{(0)}cos2\beta_1-\sigma^{(2)}2sin^2\beta_1cot\alpha_1-\sigma^{(3)}cos2\beta_1 \tag{25}$$

The stresses on the right interface of the joint can be expressed as:

$$\sigma^+=\sigma_{xx}^{(4)}+\sigma_{xx}^{(5)}=\sigma^{(4)}cos2\beta_2+\sigma^{(5)}sin2\beta_2 \tag{26}$$

$$\tau^+=\sigma_{xy}^{(4)}+\sigma_{xy}^{(5)}=\sigma^{(4)}2sin^2\beta_2cot\alpha_2-\sigma^{(5)}cos2\beta_2 \tag{27}$$

Moreover, when the incident S-wave impinges the joint, other displacement components of the transmitted wave and the reflected wave are the same as those for the incident P-wave. The particle displacement components are added to obtain the normal and tangential displacements in the x and y directions. Thus, the displacements in the left interface of the joint can be expressed as:

$$u_n^-=u^{(0)}sin\beta_1-u^{(2)}cos\alpha_1+u^{(3)}sin\beta_1 \tag{28}$$

$$u_\tau^-=-u^{(0)}cos\beta_1+u^{(2)}sin\alpha_1+u^{(3)}cos\beta_1 \tag{29}$$

The normal and tangential particle displacements on the right interface of the joint can be expressed as:

$$u_n^+=u^{(4)}cos\alpha_2+u^{(5)}sin\beta_2 \tag{30}$$

$$u_\tau^+=u^{(4)}sin\alpha_2-u^{(5)}cos\beta_2 \tag{31}$$

2.3 Time Domain Recursive Equations for the Incident P-Wave and S-Wave

In this study, the displacement discontinuity model is selected as the boundary condition. Thus, the stress satisfies $\sigma^-=\sigma^+=\sigma$ and $\tau^-=\tau^+=\tau$, and the displacement satisfies $u_n^--u_n^+=\sigma/K_n$ and $u_\tau^--u_\tau^+=\sigma/K_s$. The linear constitutive relationship is applied in the tangential direction, while the nonlinear constitutive relationship, i.e., BB model, is applied in the normal direction. Therefore, according to Eqs. (9)-(11), for an incident P-wave the stresses at the two interfaces of the joint satisfy:

$$\begin{aligned}&\sigma^{(1)}cos2\beta_1+\sigma^{(2)}cos2\beta_1-\sigma^{(3)}sin2\beta_1\\&=\sigma^{(4)}cos2\beta_2+\sigma^{(5)}sin2\beta_2\end{aligned} \tag{32}$$

$$\begin{aligned}&\sigma^{(1)}2sin^2\beta_1cot\alpha_1-\sigma^{(2)}2sin^2\beta_1cot\alpha_1-\sigma^{(3)}cos2\beta_1\\&=\sigma^{(4)}2sin^2\beta_2cot\alpha_2-\sigma^{(5)}cos2\beta_2\end{aligned} \tag{33}$$

As the rocks on the left and right of the joint have different properties, the wave impedances of the rock before and after the joint are different, i.e.,

$$Z_{P1}=\rho_1C_{P1}, Z_{P2}=\rho_2C_{P2}, Z_{S1}=\rho_1C_{S1}, Z_{S2}=\rho_2C_{S2}, \tag{34}$$

where Z_{P1} and Z_{S1} are the P-wave and S-wave impedances of the rock before the joint, respectively; Z_{P2} and Z_{S2} are the P-wave and S-wave impedances of the rock after the joint, respectively; ρ and C are the corresponding density and wave speed, respectively. From the conservation of the momentum, there is:

$$\sigma=\rho Cv \tag{35}$$

Substituting Eqs.(34) and (35) into Eqs.(32) and (33), and rewriting Eqs.(32) and (33) in matrix forms, there is

$$\begin{bmatrix}v_{(i)}^{(2)}\\v_{(i)}^{(3)}\end{bmatrix}=-B^{-1}Av_{(i)}^{(1)}+B^{-1}C\begin{bmatrix}v_{(i)}^{(4)}\\v_{(i)}^{(5)}\end{bmatrix} \tag{36}$$

where,

$$A=\begin{bmatrix} Z_{P1}cos2\beta_1 \\ Z_{P1}\left(2sin^2\beta_1 cot\alpha_1\right) \end{bmatrix} \tag{37}$$

$$B=\begin{bmatrix} Z_{P1}cos2\beta_1 & -Z_{S1}sin2\beta_1 \\ -Z_{P1}\left(2sin^2\beta_1 cot\alpha_1\right) & -Z_{S1}cos2\beta_1 \end{bmatrix} \tag{38}$$

$$C=\begin{bmatrix} Z_{P2}cos2\beta_2 & Z_{S2}sin2\beta_2 \\ Z_{P2}\left(2sin^2\beta_2 cot\alpha_2\right) & -Z_{S2}cos2\beta_2 \end{bmatrix} \tag{39}$$

The difference of the displacement on the left and right interfaces of the joint is just the deformation of the joint. Thus, there is:

$$u^{(1)}cos\alpha_1 - u^{(2)}cos\alpha_1 + u^{(3)}sin\beta_1 - u^{(4)}cos\alpha_2 - u^{(5)}sin\beta_2 = d_n \tag{40}$$

Substituting the BB model into Eq. (40) gives,

$$u^{(1)}cos\alpha_1 - u^{(2)}cos\alpha_1 + u^{(3)}sin\beta_1 - u^{(4)}cos\alpha_2 - u^{(5)}sin\beta_2 = \frac{\sigma}{k_{ni} + \sigma/d_{ma}} \tag{41}$$

When Eq. (41) is differentiated to time t, there is:

$$v^{(1)}cos\alpha_1 - v^{(2)}cos\alpha_1 + v^{(3)}sin\beta_1 - v^{(4)}cos\alpha_2 - v^{(5)}sin\beta_2 = \frac{\partial\sigma}{\partial t}\frac{k_{ni}}{\left(k_{ni} + \sigma/d_{ma}\right)^2} \tag{42}$$

Defining the normal joint stiffness $K_n = \left(k_{ni} + \sigma/d_{ma}\right)^2/k_{ni}$, where k_{ni} and d_{ma} is the initial joint stiffness and the joint maximum closure. Replacing the derivative with the differential expression:

$$v^{(1)}cos\alpha_1 - v^{(2)}cos\alpha_1 + v^{(3)}sin\beta_1 - v^{(4)}cos\alpha_2 - v^{(5)}sin\beta_2 = \frac{\sigma_{(i+1)} - \sigma_{(i)}}{\Delta t}\frac{1}{K_n} \tag{43}$$

Due to continuous stress boundary condition, it is feasible that either σ^- or σ^+ is substituted into Eq. (43). However, for simplifying the calculation, Eq. (26) is substituted into Eq. (43). After combination and reduction, there is:

$$\begin{aligned} &Z_{P2}cos2\beta_2 v_{(i+1)}^{(4)} + Z_{S2}sin2\beta_2 v_{(i+1)}^{(5)} \\ &= Z_{P2}cos2\beta_2 v_{(i)}^{(4)} + Z_{S2}sin2\beta_2 v_{(i)}^{(5)} + K_n\Delta t cos\alpha_1 v_{(i)}^{(1)} - K_n\Delta t cos\alpha_1 v_{(i)}^{(2)} \\ &+ K_n\Delta t sin\beta_1 v_{(i)}^{(3)} - K_n\Delta t cos\alpha_2 v_{(i)}^{(4)} - K_n\Delta t sin\beta_2 v_{(i)}^{(5)} \end{aligned} \tag{44}$$

In the tangential direction, there is similar relationship between the displacement and the shear stress, that is,

$$u^{(1)}sin\alpha_1 + u^{(2)}sin\alpha_1 + u^{(3)}cos\beta_1 - u^{(4)}sin\alpha_2 + u^{(5)}cos\beta_2 = \frac{\tau}{K_s} \tag{45}$$

Eq. (45) is differential to time t. And then Eq. (27) is substituted into Eq. (45). After combination and reduction, there is,

$$\begin{aligned} &Z_{P2}\left(2sin^2\beta_2 cot\alpha_2\right)v_{(i+1)}^{(4)} - Z_{S2}cos2\beta_2 v_{(i+1)}^{(5)} \\ &= Z_{P2}\left(2sin^2\beta_2 cot\alpha_2\right)v_{(i)}^{(4)} - Z_{S2}cos2\beta_2 v_{(i)}^{(5)} + K_s\Delta t v_{(i)}^{(1)}sin\alpha_1 + K_s\Delta t v_{(i)}^{(2)}sin\alpha_1 \\ &+ K_s\Delta t v_{(i)}^{(3)}cos\beta_1 - K_s\Delta t v_{(i)}^{(4)}sin\alpha_2 + K_s\Delta t v_{(i)}^{(5)}cos\beta_2 \end{aligned} \tag{46}$$

Eqs. (44) and (46) can be expressed in matrix forms as:

$$\begin{bmatrix} v_{(i+1)}^{(4)} \\ v_{(i+1)}^{(5)} \end{bmatrix} = C^{-1}H(K_n)Dv_{(i)}^{(1)} + C^{-1}H(K_n)E\begin{bmatrix} v_{(i)}^{(2)} \\ v_{(i)}^{(3)} \end{bmatrix} + \left(C^{-1}H(K_n)F + I\right)\begin{bmatrix} v_{(i)}^{(4)} \\ v_{(i)}^{(5)} \end{bmatrix} \tag{47}$$

$$D=\begin{bmatrix} \Delta t cos\alpha_1 \\ K_s\Delta t sin\alpha_1 \end{bmatrix} \tag{48}$$

$$E=\begin{bmatrix} -\Delta t cos\alpha_1 & \Delta t sin\beta_1 \\ K_s\Delta t sin\alpha_1 & K_s\Delta t cos\beta_1 \end{bmatrix} \tag{49}$$

$$F=\begin{bmatrix} -\Delta t cos\alpha_2 & -\Delta t sin\beta_2 \\ -K_s\Delta t sin\alpha_2 & K_s\Delta t cos\beta_2 \end{bmatrix} \tag{50}$$

$$H(K_n)=\begin{bmatrix} K_n & 0 \\ 0 & 1 \end{bmatrix} \tag{51}$$

$$I=\begin{bmatrix} 1 & 0 \\ 0 & 1 \end{bmatrix} \tag{52}$$

For the incident S-wave, the analysis similar to that for the incident P-wave is performed to obtain the recursive equations. The recursive equations in matrix forms are the same as those for the incident P-wave, while matrix *A* and matrix *D* for the incident S-wave are different with those for the incident P-wave. The matrix *A* and matrix *D* for the incident S-wave are:

$$A=\begin{bmatrix} Z_{S1}sin2\beta_1 \\ -Z_{S1}cos2\beta_1 \end{bmatrix} \tag{53}$$

$$D=\begin{bmatrix} \Delta t sin\beta_1 \\ -K_s\Delta t cos\beta_1 \end{bmatrix} \tag{54}$$

3. SPCICAL CASES

When the incident P-wave is perpendicular to the joint, there is $\alpha_1 = 0$. From Snell's law, other emitted angles are zero, i.e., $\beta_1 = \alpha_2 = \beta_2 = 0$. Substituting the expression into the matrices from A to F yields,

$$A=\begin{bmatrix} Z_{P1} \\ 0 \end{bmatrix} \tag{55}$$

$$B=\begin{bmatrix} Z_{P1} & 0 \\ 0 & -Z_{S1} \end{bmatrix} \tag{56}$$

$$C=\begin{bmatrix} Z_{P2} & 0 \\ 0 & -Z_{S2} \end{bmatrix} \tag{57}$$

$$D=\begin{bmatrix} \Delta t \\ 0 \end{bmatrix} \tag{58}$$

$$E=\begin{bmatrix} -\Delta t & 0 \\ 0 & K_s\Delta t \end{bmatrix} \tag{59}$$

$$F=\begin{bmatrix} -\Delta t & 0 \\ 0 & K_s\Delta t \end{bmatrix} \tag{60}$$

It should be noted that in the expressions "$2sin^2\beta_1 cot\alpha_1$" and "$2sin^2\beta_1 cot\alpha_1$" cotangent values of α_1 or α_2 are nonexistent when $\alpha_1=\alpha_2=0$. In fact, their transitory expressions are "$(C_S/C_P)^2 sin2\alpha$", i.e., $(C_S/C_P)^2 sin2\alpha=2sin^2\beta cot\beta$. Thus, when α is equal to 0, the expression "$(C_S/C_P)^2 sin2\alpha$" is used to calculate the matrices. Substituting the simplified matrices from A to C into Eq. (36), there is:

$$\begin{bmatrix} Z_{P1}v_{(i)}^{(2)} \\ -Z_{S1}v_{(i)}^{(3)} \end{bmatrix} = -\begin{bmatrix} Z_{P1}v_{(i)}^{(1)} \\ 0 \end{bmatrix} + \begin{bmatrix} Z_{P2}v_{(i)}^{(4)} \\ -Z_{S2}v_{(i)}^{(5)} \end{bmatrix} \tag{61}$$

After the simplification, there are,

$$Z_{P1}\left(v_{(i)}^{(2)}+v_{(i)}^{(1)}\right)=Z_{P2}v_{(i)}^{(4)} \tag{62}$$

$$v_{(i)}^{(3)}=v_{(i)}^{(5)}=0 \tag{63}$$

Eq. (62) indicates that the stresses on the left and right interfaces of the joint are continuous. When the rock properties on the two interfaces of the joint are the same, i.e., $Z_{P1}=Z_{P2}$, there is,

$$v_{(i)}^{(2)}+v_{(i)}^{(1)}=v_{(i)}^{(4)}. \tag{64}$$

Eqs. (63) and (64) are the same form as previously derived equations by Zhu and Zhao (2013). Also, the simplified matrices from D to F are substituted into Eq. (47), and the equations in matrix form can be rewritten as:

$$\begin{bmatrix} Z_{P2}v_{(i+1)}^{(4)} \\ -Z_{S2}v_{(i+1)}^{(5)} \end{bmatrix} = \begin{bmatrix} -K_n \Delta t v_{(i)}^{(2)} \\ K_s \Delta t v_{(i)}^{(3)} \end{bmatrix} + \begin{bmatrix} (-K_n \Delta t + Z_{P2})v_{(i)}^{(4)} \\ (K_s \Delta t - Z_{S2})v_{(i)}^{(5)} \end{bmatrix} + \begin{bmatrix} K_n \Delta t v_{(i)}^{(1)} \\ 0 \end{bmatrix} \tag{65}$$

Substituting Eq. (62) into Eq. (65) and simplifying them gives:

$$v_{(i+1)}^{(4)}=-K_n \Delta t \left(\frac{1}{Z_{P1}}+\frac{1}{Z_{P2}}\right)v_{(i)}^{(4)}+v_{(i)}^{(4)}+\frac{2K_n \Delta t}{Z_{P2}}v_{(i)}^{(1)} \tag{66}$$

where $K_n=\left(k_{ni}+\dfrac{Z_{P2}v_{(i)}^{(4)}}{d_{ma}}\right)^2 \Big/ k_{ni}$

Eqs. (62) and (66) are similar to the previously derived equations by Fan et al. (2018). In the equation derived by L.F.Fan, the joint stiffness is constant. Thus, the equation is the special case when the stress wave is perpendicular to the linearly elastic joint. When the rock properties before and after the joint are the same, i.e., $Z_{P1}=Z_{P2}$, Eq.(66) can be simplified as:

$$v_{(i+1)}^{(4)}=v_{(i)}^{(4)}+\frac{2K_n \Delta t}{Z_P}\left(v_{(i)}^{(1)}-v_{(i)}^{(4)}\right) \tag{67}$$

Eq.(67) is also the same as the equation derived by Li and Ma (2010). Similarly, for the normal incident S-wave, matrix A and matrix D are simplified as:

$$A=\begin{bmatrix} 0 \\ -Z_{S1} \end{bmatrix} \tag{68}$$

$$D=\begin{bmatrix} 0 \\ -K_s \Delta t \end{bmatrix} \tag{69}$$

In order to obtain the S-wave recursive equations for the special case, what needed to do is to replace Eqs. (55) and (58) with Eqs. (68) and (69) for all the P-wave recursive equations, and to replace $v_{(i)}^{(1)}$ with $v_{(i)}^{(0)}$, respectively. Thus, there are,

$$Z_{S1}\left(v_{(i)}^{(3)}+v_{(i)}^{(0)}\right)=Z_{S2}v_{(i)}^{(5)} \tag{70}$$

$$v_{(i)}^{(2)}=v_{(i)}^{(4)}=0 \tag{71}$$

$$v_{(i+1)}^{(5)}=-K_s \Delta t \left(\frac{1}{Z_{S1}}+\frac{1}{Z_{S2}}\right)v_{(i)}^{(5)}+v_{(i)}^{(5)}+\frac{2K_s \Delta t}{Z_{S2}}v_{(i)}^{(0)} \tag{72}$$

When the rock properties before and after the joint are the same, i.e., $Z_{S1}=Z_{S2}=Z_S$, Eq.(72) can be simplified as:

$$v_{(i+1)}^{(5)}=v_{(i)}^{(5)}+\frac{2K_s \Delta t}{Z_s}\left(v_{(i)}^{(0)}-v_{(i)}^{(5)}\right) \tag{73}$$

Eq.(73) is also the same as the equation derived by Li and Ma (2010).

4. COMPARISON AND VERIFICATION

4.1 A Comparison with the Results by Zhao J

In order to verify the derived wave equations, a comparison with the conclusion given by Zhao and Cai (2001) is conducted. The same parameters are selected from the reference (Zhao and Cai, 2001). The parameters are listed in Table 1.

Table 1 Rock parameters

Rock density (kg/m³)	2400
P-wave speed(m/s)	4500
Particle velocity amplitude(m/s)	0.1,0.02
Wave frequency(Hz)	50
Initial normal joint stiffness (GPa/m)	1.25
Maximum allowable closure(mm)	0.61

The calculated results are shown in Figure 2. Figure 2(a) and Figure 2(b) illustrate a half-cycle sinusoidal incident wave and the corresponding transmitted wave, respectively. From them, when the joints are impinged by the incident wave with the amplitude of 0.1 m/s and 0.02 m/s, the transmitted waves derived in the present study are both close to those given by Zhao and Cai (2001).
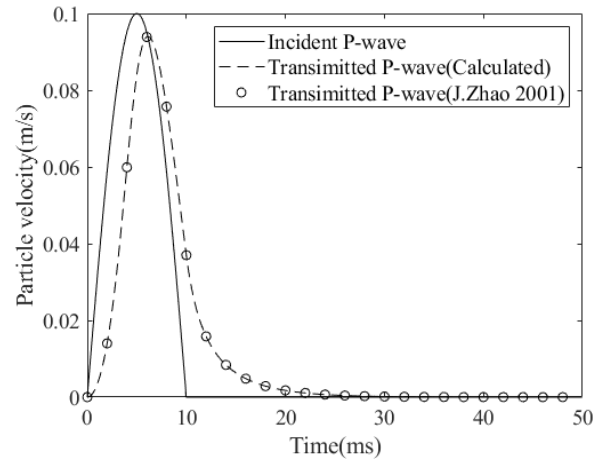


(a) when the incident wave peak equals 0.1 m/s
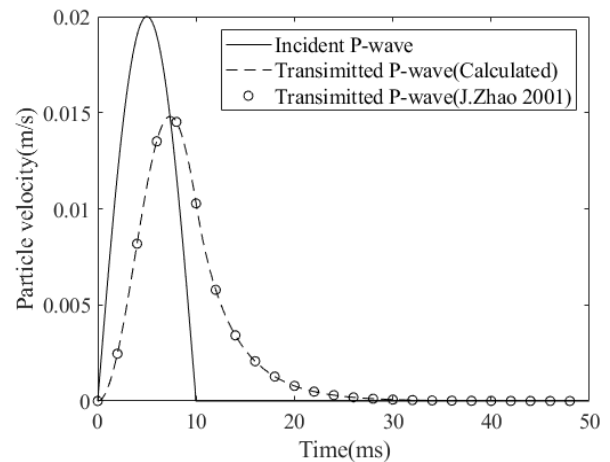
(b) when the incident wave peak equals 0.02 m/s
Figure 2 A comparison of the results given by Zhao with the calculated data
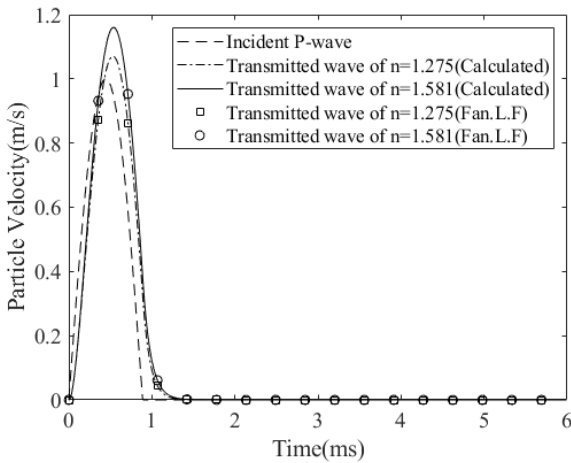
4.2 A Comparison with the Results by Fan L F

Fan et al. (2018) investigated the wave propagation through the jointed complex rock masses when the P-wave is perpendicular to the joint. The present study attempts to study the wave across the jointed complex rock masses with arbitrary incident angles. In order to verify

the wave equations derived in the present study, another comparison between the results derived in the present study and those by Fan et al. (2018) is conducted. The parameters adopted here are the same as those in the reference (Zou et al., 2016). Figure 3 illustrates the particle velocity transmission waves when the incident wave propagates through the joint from the "soft" rock to the "hard" rock, i.e., the wave impedance ratios n = 0.306 and 0.408. Figure 4 shows the particle velocity transmission waves when the incident wave propagates through the "hard-to-soft" rock masses, i.e., the wave impedance ratios n = 1.275 and 1.581. From the two figures, the particle velocities of transmission waves calculated in the present study agree with those in the reference (Fan et al., 2018).
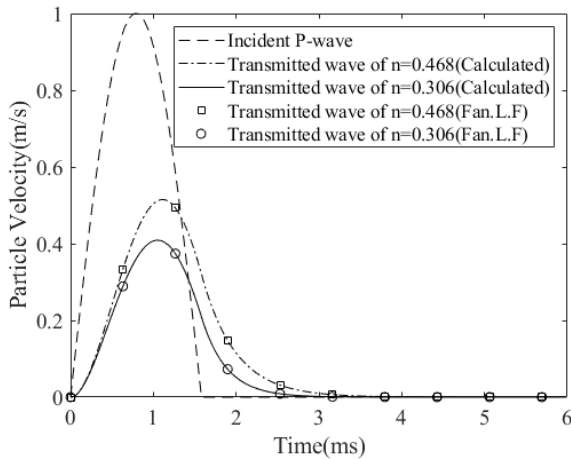
(a) wave impedance ratios less than 1

(b) wave impedance ratios greater than 1

Figure 3 A comparison of the particle velocity waves derived by Fan.L.F with the calculated results

Therefore, the wave equations derived in the present study are correct and effective. And the MTDRM is effective and feasible to investigate the wave across the jointed complex rock masses. The effect of the wave impedance ratios on the transmission and reflection coefficients of the particle velocity wave with the different incident angles will be discussed in the following sections.

5. WAVE PROPAGATION ACROSS THE JOINTED COMPLEX ROCK MASSESS WITH ARBITRARY INCIDENT ANGLES

5.1 The Rock Mass Parameters and the Boundary Conditions

In the present study, the parameters same as those in reference (Fan et al., 2018) are applied. A half-cycle sinusoidal is assumed to be incident on the jointed complex rock masses with arbitrary angles. The wave amplitude is 1.0 m/s, and the frequency is set to be 316.2 Hz, and the initial normal and tangential joint stiffness are both

8.0 GPa/m. Poisson's ratio of the intact rock is 0.2. BB model and the linearly elastic model are chosen as the normal and tangential joint constitutive relationship, respectively. For the rocks at the left and right of the joint, their Young's moduli and volume densities are listed in Table 2. To discuss the wave propagation across the "soft-to-hard" rock masses, Rock III from Table 2 is selected for the rock at the right of the joint, while Rock I and Rock II are selected for the rock at the left of the joint. Thus, the wave impedance ratios are 0.306 and 0.408, respectively. In addition, to discuss the wave propagation through the "hard-to-soft" rock masses, Rock III from Table 2 is selected for the rock at the right of the joint, while Rock IV and Rock V are selected for the rock at the left of the joint. Thus, the wave impedance ratios are 1.275 and 1.581, respectively. For the rock before and after the joint which has the same property, the parameters of Rock III are selected for the rock before and after the joint. Thus, the wave impedance ratio is 1. In this case the jointed complex rock masses are degenerated into the jointed simple rock masses discussed in the previous study.

Table 2 Parameters of the intact rocks

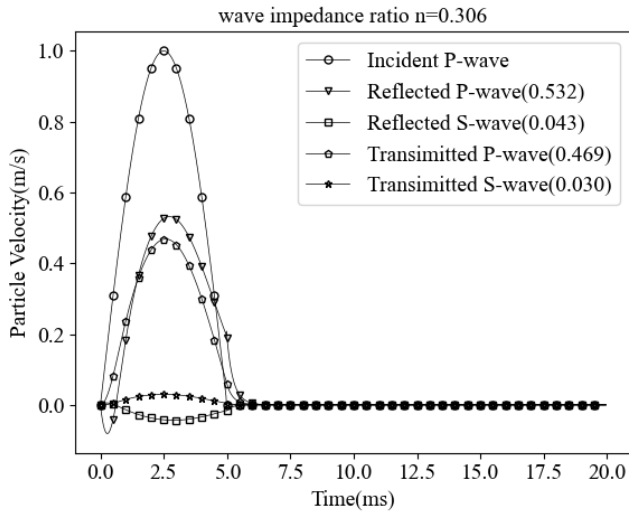|	Rock I	Rock II	Rock III	Rock IV	Rock V
E(GPa)	5	10	40	60	80
ρ (kg/m³)	1800	2100	2400	2600	3000

5.2 Wave Propagation Through the Jointed Complex Rock Masses

When the effects of the wave impedance ratios on the wave propagation are investigated, in order to reduce the disturbance from the incident angle, it is the most appropriate way that the incident angle is set to 0. However, the normal incident P-wave cannot trigger the reflected and transmitted S-wave and the normal incident S-wave cannot trigger the reflected and transmitted P-wave. Thus, a relatively small incident angle $\alpha = 2°$ is selected for P-wave and S-wave. From Eqs. (36) and (47), when the P-wave and S-wave with the incident angle of 2° interact with the joint, the corresponding transmitted and reflected P-wave and S-wave are calculated. The results are shown in Figure 4 and Figure 5. In the figures the numbers in parentheses are the transmitted or reflected coefficients.
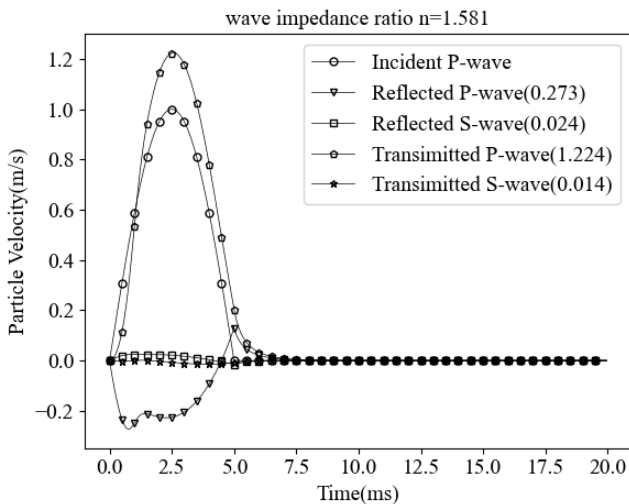
Figure 4(a) illustrates the wave propagation when the incident P-wave propagates crossing the joint from the "soft" rock to the "hard" rock. Figure 4(b) shows the wave propagation when the incident P-wave impinges the joint from the "hard" rock to the "soft" rock. In Figure 4(a) and Figure 4(b), the transmitted and reflected coefficients of the transmitted S-wave and reflected S-wave are 0.030, 0.043 and 0.014, 0.024, respectively. The coefficients are very small. It is because that the P-wave incident angle is selected to be 2° and the angle is tiny. Thus, the little incident P-wave energy converts into the transmitted and reflected S-wave energy by the wave mode conversion. In Figure 4(b), when the wave impedance ratio is 1.581, the transmission coefficient of the transmitted P-wave is 1.224. The transmitted coefficients surpass 1. Obviously the transmitted P-wave has larger amplitude than the incident P-wave. It shows that the incident P-wave crossing the joint from the "hard" rock to the "soft" rock is enlarged.

Figure 5(a) and Figure 5(b) show the particle velocity wave propagations when the incident S-wave passes through the "soft-to-hard" and "hard-to-soft" rock masses, respectively. In Figure 5, the coefficients of the transmitted and reflected P-wave are 0.030, 0.044 and 0.011, 0.033. The transmission and reflection coefficients of the corresponding P-wave are small compared to those of the other velocity waves. Similar to the case for the incident P-wave, for the incident S-wave the smaller incident angle also results in less wave mode conversion. Moreover, when the wave impedance ratio n = 1.581, the transmission coefficient of the transmitted S-wave for the incident S-wave is 1.175. The coefficient is greater than 1. It indicates that the transmitted S-wave is enhanced when S-wave propagates through the jointed rock with the large wave impedance

ratio. For the case that wave propagates through the "hard-to-soft" jointed rock masses, when P-wave is selected as the incident wave, the transmitted P-wave is enlarged, and when S-wave is selected as the incident wave, the transmitted S-wave is enlarged. Thus, the enlarged transmitted wave is usually the wave whose wave type is the same as that of the incident wave.
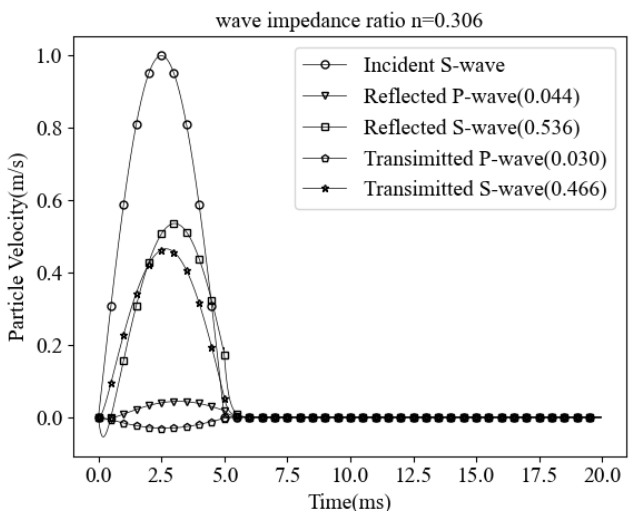
wave impedance ratio n=0.306

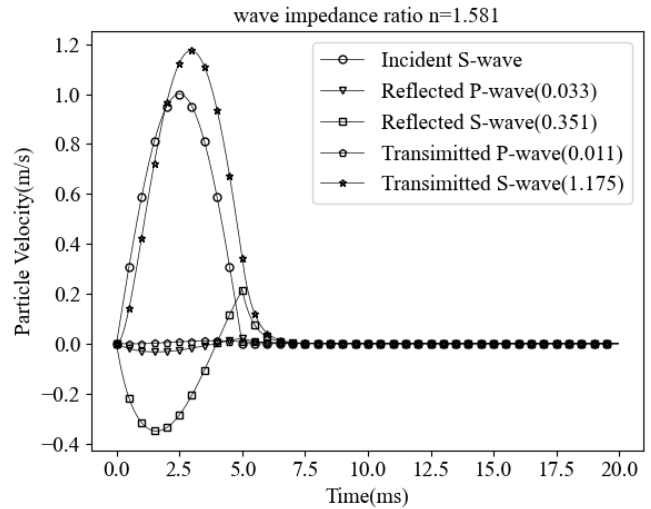Incident P-wave
Reflected P-wave(0.532)
Reflected S-wave(0.043)
Transimitted P-wave(0.469)
Transimitted S-wave(0.030)

(a) when wave impedance n = 0.306

wave impedance ratio n=1.581

Incident P-wave
Reflected P-wave(0.273)
Reflected S-wave(0.024)
Transimitted P-wave(1.224)
Transimitted S-wave(0.014)

(b) when wave impedance n = 1.581
Figure 4 Transmission and reflection wave for an incident P-wave

wave impedance ratio n=0.306

Incident S-wave
Reflected P-wave(0.044)
Reflected S-wave(0.536)
Transimitted P-wave(0.030)
Transimitted S-wave(0.466)

(a) when the wave impedance ratio n = 0.306

wave impedance ratio n=1.581

Incident S-wave
Reflected P-wave(0.033)
Reflected S-wave(0.351)
Transimitted P-wave(0.011)
Transimitted S-wave(1.175)

(b) when the wave impedance ratio n = 1.581
Figure 5 The transmission and reflection wave for an incident S-wave

6. PARAMETRIC STUDIES AND DISCUSSION

6.1 The Effect of the Wave Impedance Ratios on the Transmission and Reflection Coefficients

In order to fully understand the incident P-wave and S-wave with the different angles propagation through the jointed complex rock masses, seven angles, i.e., 0°, 2°, 4°, 6° ,8°, 10°, and 12°, are selected as the incident angles, and five wave impedance ratios, i.e., 0.306, 1.468, 1.0, 1.275, and 1.581, are applied.

### 6.1.1 The Case for the Incident P-Wave

To characterize three kinds of rock masses, that is, the "soft-to-hard" rock masses, the "hard-to-soft" rock masses and the conventional simple rock masses, and then the effects of the angles and wave impedance ratios on the transmission and reflection coefficients are discussed.

Figure 6 illustrates the relation between the wave impedance ratios and particle velocity transmission and reflection coefficients with the different P-wave incident angles. From Figure 6(a), it can be seen that the reflected P-wave coefficients decrease firstly and then increase with the increasing of wave impedance ratios. When the wave impedance ratio is 1, the reflected P-wave coefficients reach the minimum. Moreover, with the increase of the incident angles of P-wave, the P-wave reflection coefficients decrease gradually.

In Figure 6(b), there is not the reflected S-wave when P-wave is perpendicular to the joint. Thus, the corresponding reflected coefficient can be considered to be 0. It can be seen from Figure 6(b) that the changing trends of the S-wave reflection coefficients with the variation of the wave impedance ratios are not monotonous. Similar to Figure 6(a), the trends decease firstly and then increase. The reflection coefficients reach peak when the wave impedance ratio is 1. That the wave impedance ratio equals 1 means that the rock before and after the joint has the same property. The rock masses are degenerated into the jointed simple rock masses discussed in the previous study. In other word, the reflection coefficients of the reflect S-wave get minimum when the incident P-wave interacts with jointed simple rock masses. In addition, when the incident angles increase from 0° to 12°, the reflected coefficients of the reflected S-wave increase gradually.

From Figure 7(a), no matter what value the incident angles are, the particle velocity transmission coefficients of the transmitted P-wave increase with the increasing of the wave impedance ratios, and the relation between two parameters is monotonous. In this figure, seven curved lines charactering the relations between the transmitted coefficients and the wave impedance ratios with the different incident angles intersect, which indicates that for the case the effects of the

14

incident angles on the transmission coefficients are relatively small. Also, it is interesting that the transmission coefficients of the transmitted P-wave is greater than 1 when the wave impedance ratio is larger than 1. It indicates that the amplitude of the transmitted P-wave surpasses that of the incident wave when P-wave propagates across the "hard-to-soft" jointed rock masses with the incident angles from 0° to 12°.
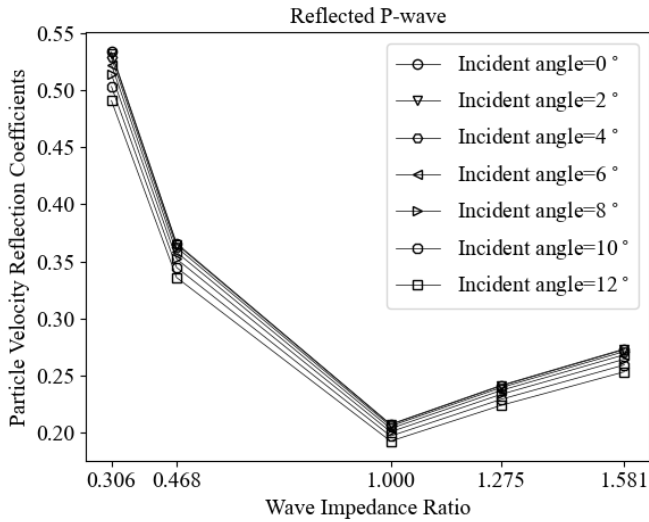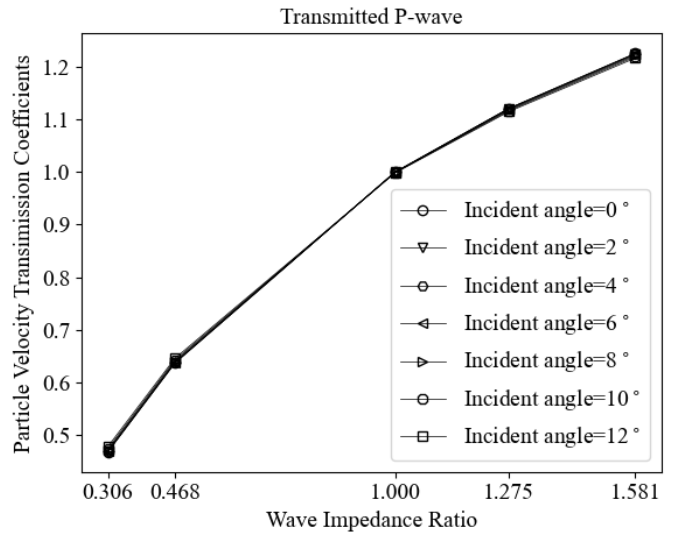

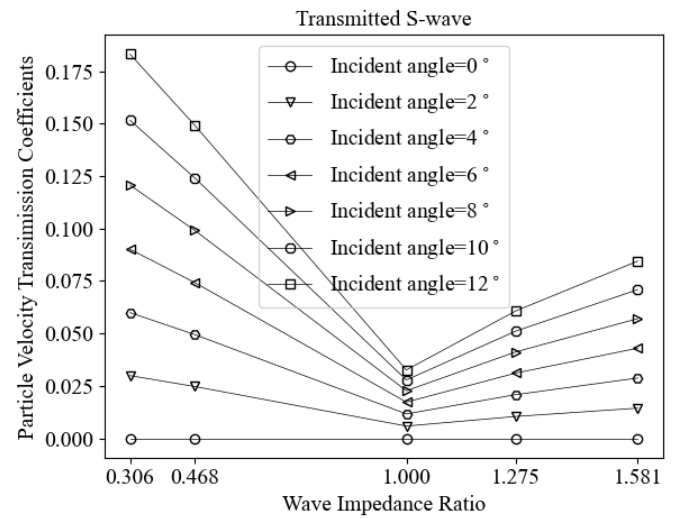(a) for the reflected P-wave
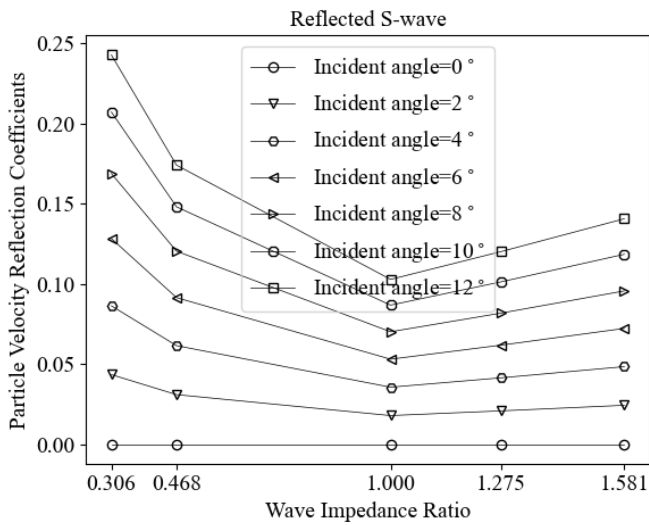
(b) for the reflected S-wave

Figure 6 The effect of the wave impedance ratios on the reflection coefficients for an incident P-wave

Figure 7(b) shows the effect of the wave impedance ratios on the transmission coefficients of the transmitted S-wave with the various incident angles. When the wave impedance ratios change from 0.306 to 1.581, i.e., the rock medium changing from the "soft-to-hard" rock masses to the "hard-to-soft" rock masses, the transmission coefficients reach the trough firstly and then grow up. Also, the effect of the incident angles on the transmission coefficients of transmitted S-wave is greater than those of the transmitted P-wave illustrated in Figure 7(a).

In Figures 6(a) and 7(a), when P-wave interacts with the joint , the coefficients of transmitted P-wave and reflected P-wave change less with the changing of the incident angles; on the contrary, the coefficients of transmitted P-wave and reflected P-wave change sharply with the increasing of the wave impedance ratios., it seems that for the case of P-wave incident on the joint wave impedance ratios have greater influence on the coefficients of transmitted P-wave and reflected P-wave than the incident angles.

(a) for the transmitted P-wave
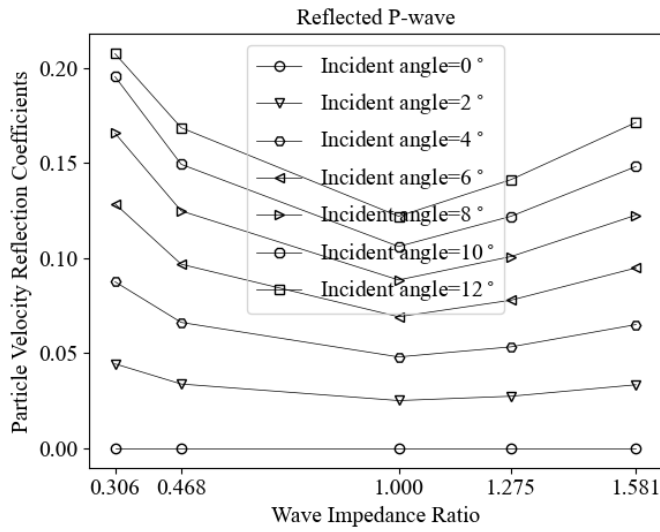

(b) for the transmitted S-wave

Figure 7 The effect of the wave impedance ratios on the transmission coefficients for an incident P-wave

### 6.1.2 The Case for the Incident S-Wave

Figures 8(a) and 8(b) illustrate the relations between the reflection coefficients of the reflected P- and S-wave and the wave impedance ratios. With the wave impedance ratios increasing from 0.306 to 1.581, the reflection coefficients of the reflected P- and S-wave increase firstly and then decrease except that the changing trend has slight difference when the incident angle = 12°. When the wave impedance ratio is 1, the reflected coefficients of P-wave and S-wave reach the minimum. However, compared with the coefficients of the reflected P-wave, the coefficients of the reflected S-wave decrease in relatively high speed when the wave impedance ratios increase from 0.306 to 1, and also rise more rapidly when the wave impedance ratios vary from 1 to 1.581. It indicates that for a same incident angle the effects of the wave impedance ratios on the reflection coefficients of the reflected S-wave are greater than those of the reflected P-wave. Furthermore, Figure 8(b) shows that for the same wave impedance ratios, the effects of the incident angles on the reflected coefficients are larger and larger when the incident angles increase from 0° to 12°.

Figure 9(a) illustrates the changing trends that the transmission coefficients of the transmitted P-wave increase with the wave impedance ratio increasing. With the wave impedance ratio increasing from 0.306 to 1, the transmission coefficients decrease sharply, and then increase in a slight speed when impedance ratios increase from 1 to 1.581. The coefficient increments are very small

and nearly negligible when impedance ratios increase from 1 to 1.581. It shows that the wave impedance ratios have a slight influence on the transmission coefficients of the transmitted P-wave when S-wave propagates through the "hard-to-soft" rock masses.

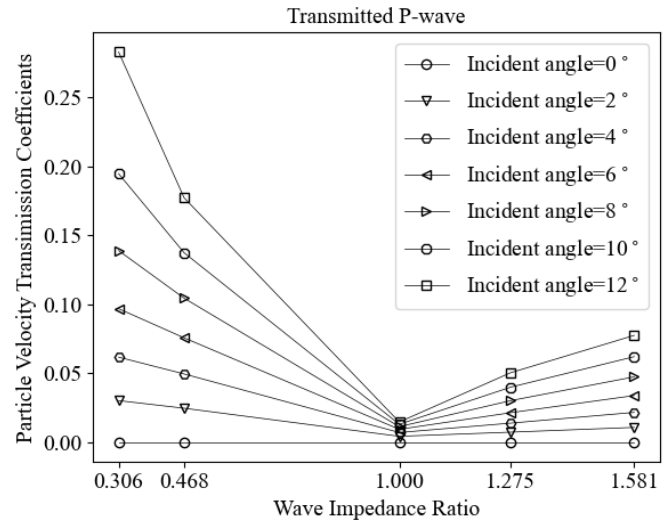(a)   for the reflected P-wave
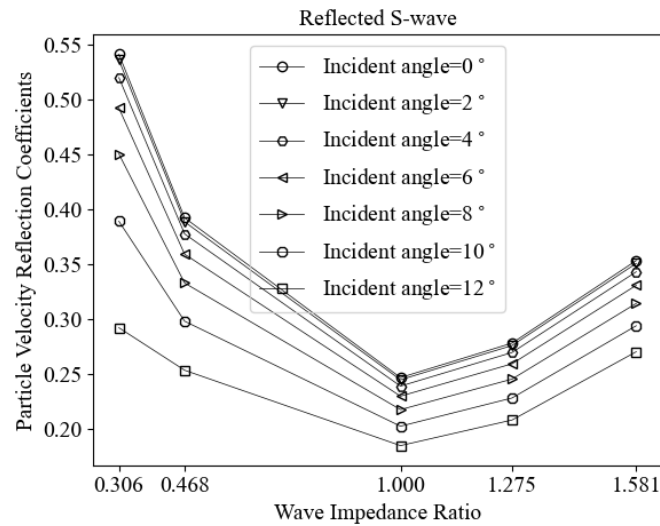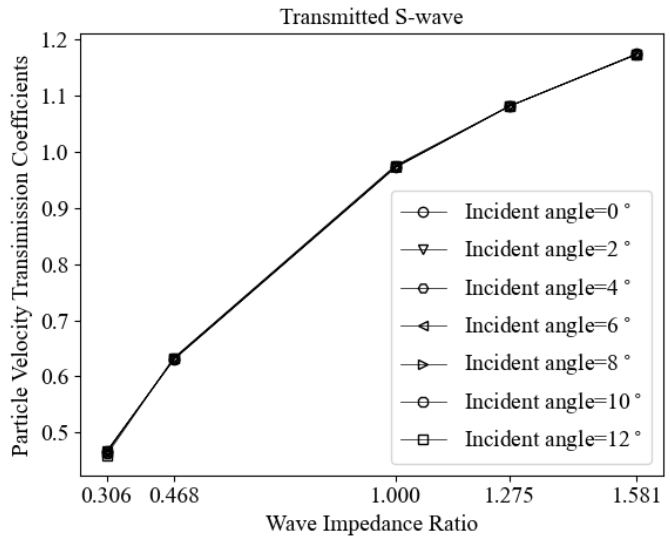

(b) for the reflected S-wave

Figure 8 The effect of the wave impedance ratios on the reflection coefficients for an incident S-wave

Figure 9(b) shows how the transmission coefficients of the transmitted S-wave are influenced by the wave impedance ratios when the different incident angles are selected. In this figure, the changing trends of the transmitted coefficients are very similar for the different incident angles. It seems that the changings of the incident angles have a negligible influence on the transmission coefficients. However, the transmission coefficients of the transmitted S-wave fast monotonously increase with the increasing of the wave impedance ratios. The wave impedance ratios have larger effect on the transmission coefficients than the incident angles.

In all, whether the jointed rock masses is "soft-to-hard" or "hard -to- soft" rock masses has obvious influence on the transmission wave. Especially, the transmission wave induced by the incident wave of the same type, i.e., the transmission P-wave triggered by the incident P-wave and the transmission S-wave triggered by the incident S-wave, has sensitive response on the changing wave impedance ratio. And the transmission wave induced by the incident wave crossing the "hard -to- soft" jointed rock masses is strengthened.

(a) for the transmitted P-wave

(b) for the transmitted S-wave

Figure 9 The effect of the wave impedance ratios on the transmission coefficients for an incident S-wave

7.   CONCLUSIONS

In the present study, a modified time domain recursive method (MTDRM) is presented. The stresses and particle velocities caused by interaction of the P-wave and S-wave at an arbitrary incident angle with the jointed complex rock masses are analyzed. The wave equations across a jointed complex rock masses joint are established by introducing BB model and the displacement discontinuity model. After the equations are degenerated, it is found that the wave propagation across the conventional jointed rock masses is a special case when the wave impedance ratios of the equations in the present study are set to 1.0 and the incident angle is equal to 0. A comparison with the previous research shows that the MTDRM is effective and feasible to investigate the transmission and reflection of P-wave and S-wave crossing the joint at an arbitrary incident angle.

The two cases, i.e., wave propagation across the "soft-to-hard" rock masses and the "hard -to- soft" rock masses, are analyzed. And the special case that the wave propagates through the joint, before and after which the rock properties are the same, is also investigated.

For the incident P-wave, the effects of the wave impedance ratios on the coefficients of reflected P-wave, S-wave and transmitted S-wave are not monotonous. The coefficients have a minimum trough in the process of the wave impedance ratio increasing. However, the transmission coefficients of the transmitted P-wave triggered by the incident P-wave monotonously increase with the increasing of the

wave impedance ratios. Also, it is interesting that when the wave impedance ratios equal 1.275 and 1.581. i.e., wave propagation through the joint from the "hard" rock to the "soft" rock, the transmission coefficients of the transmitted P-wave is greater than 1.

When the S-wave is incident on the joint, the changing trends of the coefficients of the transmitted P-wave and the reflected P- and S-wave with the increasing of the wave impedance ratios usually have the troughs except for the transmitted S-wave. The wave impedance ratio the trough corresponds to is 1. The effects of the incident angles on the reflection coefficients of the reflected S-wave are larger and larger with the angle increasing from 0° to 12°. Also, the effects of the incident angles on the transmission coefficients of the transmitted S-wave are nearly negligible. However, the influences of wave impedance ratios on the transmission coefficients of the transmitted S-wave are obvious.

Nevertheless, it should be noted that the present study assumes that the wave is planar. The assumption is based on the precondition that the wave has propagated to the far field. If the wave propagates in the near field, the wave is spherical. Thus, that the spherical wave impinges the jointed complex rock masses will be investigated in the future.

8.　ACKNOWLEDGEMENTS

9.　REFERENCES

Bandis, S. C., Barton, N. R., and Christianson, M. (1985) "Application of a new numerical model of joint behavior to rock mechanics problems," In: Proc., Int. Symposium on Fundamentals of Rock Joints. Lulea, Sweden, pp345-356.

Bandis, S. C., Lumsden, A. C., and Barton, N. R. (1983) "Fundamentals of rock fracture deformation," International Journal of Rock Mechanics and Mining sciences, 20, Issue 6, pp249-268.

Cai, J. G., and Zhao, J., (2000) "Effects of multiple parallel fractures on apparent attenuation of stress waves in rock masses," International Journal of Rock Mechanics and Mining sciences, 37, Issue 4, pp661-682.

Che, A., Yang, H., Wang, B., and Ge, X. (2016) "Wave propagations through jointed rock masses and their effects on the stability of slopes," Engineering Geology, Issue 20, pp45-56.

Deng, X. F., Zhu, J. B., and Chen, S. G. (2014) "Numerical study on tunnel damage subject to blast-induced shock wave in jointed rock masses," Tunneling & Underground Space Technology, Issue 43, pp88-100.

Fan, L. F., Ma, G. W., Li, J. C. (2012) "Nonlinear viscoelastic medium equivalence for stress wave propagation in a jointed rock mass," International Journal of Rock Mechanics and Mining sciences, Issue 50, pp11-18.

Fan, L. F., Wang, L. J., and Wu, Z. J. (2018) "Wave transmission across linearly jointed complex rock masses," International Journal of Rock Mechanics and Mining sciences, Issue 112, pp193-200.

Fan, L. F., and Wong, L.N.Y. (2013) "Stress wave transmission across a filled joint with different loading/unloading behavior," International Journal of Rock Mechanics and Mining sciences, Issue 60, pp227–234.

Kitsunezaki, C. (1983) "Behavior of plane elastic waves across a plane crack," Journal of Mining College of Akita University, 6, Issue 3, pp173-187.

Li, J. C. (2013) "Wave propagation across non-linear rock joints based on time-domain recursive method," Geophysical Journal International, 193, Issue 2, pp970–985.

Li, J. C., and Ma, G. W. (2010) "Analysis of blast wave interaction with a rock joint," Rock Mechanics & Rock Engineering, Issue 43, pp777–787.

Li, J. C., Ma, G. W., and Zhao, J. (2010) "An equivalent viscoelastic model for rock mass with parallel joints," Journal of Geophysical Research, 115, Issue B3, pp3305-3315.

Li, Y., and Wang, J. (2019) "Effects of Porosity of Dry and Saturated Sandstone on the Energy Dissipation of Stress Wave," Advances in Civil Engineering, pp1-10.

Li, Y., Pan, H., and Qin, L. (2018) "Influence of two rough parallel joint surface profiles on stress wave energy dissipation," Geotechnical Engineering, 49, Issue 3, pp47-54.

Li, Y., and Zhu, Z. (2012) "Study on the velocity of P waves across a single joint based on fractal and damage theory," Engineering Geology, Issue 151, pp82-88.

Li, Y., Zhu, Z., and Li, B. (2011) "Study on the transmission and reflection of stress waves across joints," International Journal of Rock Mechanics and Mining sciences, 48, Issue 3, pp364-371.

Nakagawa, S., Nihei, K. T., and Myer, L. R. (2000) "Shear-induced conversion of seismic waves across single fractures," International Journal of Rock Mechanics and Mining sciences, 37, Issue 1, pp203-218.

Perino, A., Orta, R., and Barla, G. (2012) "Wave Propagation in Discontinuous Media by the Scattering Matrix Method," Rock Mechanics & Rock Engineering, Issue 45, pp901–918.

Perino, A., Zhu, J. B., Li, J. C. (2010) "Theoretical Methods for Wave Propagation across Jointed Rock Masses," Rock Mechanics & Rock Engineering, 43, Issue 6, pp799-809.

Schoenberg, M. A. (1983) "Reflection of elastic waves from periodically a stratified media with interfacial slip," Geophysical Prospecting, 31(2), pp265-292.

Song, L., Yan, Y. Z., Han, B. X. (2012) "Theoretical research into the wave propagation of P-wave across rock joint with nonlinear deformation," Chinese Journal of Applied Mechanics, 29, Issue 2, pp133-141. (in Chinese)

Wang, R., Hu, Z., and Zhang, D. (2017) "Propagation of the Stress Wave through the Filled Joint with Linear Viscoelastic Deformation Behavior Using Time-Domain Recursive Method," Rock Mechanics & Rock Engineering, Issue 50, pp3197–3207.

Zeng, S., Wang, S., and Sun, B. (2018) "Propagation Characteristics of Blasting Stress Waves in Layered and Jointed Rock Caverns," Geotechnical & Geological Engineering, Issue 36, pp1559–1573.

Zhao, J., Zhao, X. B., and Cai, J G. (2006) "A further study of P-wave attenuation across parallel fractures with linear deformational behaviour," International Journal of Rock Mechanics and Mining sciences, 43, Issue 5, pp776-788.

Zhao, J., and Cai, J. G. (2001) "Transmission of elastic P-waves across single fracture with a nonlinear normal deformational behavior," Rock Mechanics & Rock Engineering, 34, Issue 1, pp3-22.

Zhu, J. B., Zhao, X. B., and Li, J. C. (2011) "Normally incident wave propagation across a joint set with the virtual wave source method", Journal of Applied Geophysics, 73, Issue 3, pp283-288.

Zhu, J. B., and Zhao J. (2013) "Obliquely incident wave propagation across rock joints with virtual wave source method."

Zhu, J. B., Perino, A., Zhao, G. F. (2011) "Seismic response of a single and a set of filled joints of viscoelastic deformational behavior," Geophysical Journal International, 186, Issue 3, pp1315–1330.

Zou, Y., Li, J. C., Laloui, L. (2017) "Analytical Time-Domain Solution of Plane Wave Propagation Across a Viscoelastic Rock Joint," Rock Mechanics & Rock Engineering, Issue 50, pp 2731–2747.